

Coupling of Shear Acoustic Waves by Gratings: Analytical and Experimental Analysis of Spatial Periodicity Effects

T. Valier-Brasier^{1,3)}, C. Potel^{1,3)}, M. Bruneau^{1,3)}, D. Leduc^{2,3)}, B. Morvan^{2,3)}, J.-L. Izbicki^{2,3)}

¹⁾ Laboratoire d'Acoustique de l'Université du Maine (LAUM), UMR CNRS 6613, Université du Maine, Avenue Olivier Messiaen, 72 085 Le Mans Cedex 9, France. catherine.potel@univ-lemans.fr

²⁾ Laboratoire d'Ondes et Milieux Complexes, Groupe Ondes Acoustiques, FRE CNRS 3102, Université du Havre, Place Robert Schumann, BP 4006, 76 610 Le Havre, France

³⁾ Fédération Acoustique du Nord-Ouest (FANO) FR CNRS 3110

Summary

A model, presented in a previous paper [J. App. Phys. **108** (2010) 074910], describing the modes coupling due to scattering on small one-dimensional irregularities (parallel ridges) of the surface of isotropic solid plates, when shear horizontal waves polarized along the ridges propagate perpendicularly to them, appears to be a convenient tool to tackle the effects of the shape profile of the ridges (including the depth and the slope). Being concerned by the use of this analytical approach not utilised until now, several results, yet typical of applications, are presented below and compared with some experimental and numerical results, even analytical results (from an alternative analytical model for particular cases). These comparisons permit to highlight the effects of spatial periodicities of the ridges and show that the method could provide information on geometrical parameters characterising the profile of the roughness, which could be of interest when other methods like optical methods cannot be used.

PACS no. 43.20.-f, 43.20.Ef, 43.20.Fn, 43.35.-c, 43.35.Cg

1. Introduction

The paper aims at providing results obtained from both an analytical model presented in a previous paper [1] and an experimental setup installed for the purpose [2], in order to describe the modes coupling due to scattering on small one-dimensional irregularities (parallel ridges) of the surface of isotropic solid plates, when shear horizontal waves polarized along the ridges propagate perpendicularly to them, having in mind to propose a convenient method to tackle the effects of the shape profile of the ridges (including the depth and the slope).

The two-dimensional (x, z) , homogeneous solid plate in vacuum [domain (D) , $z \in (z_1, z_2)$] considered, is assumed to be infinite in the y -direction and bounded by two parallel surfaces perpendicular to the z -axis, one of them having 1D shape perturbation (small ridges parallel to the y -axis) (Figure 1). At the entrance $x = 0$ of this plate, a harmonic, incident propagating SH-wave (speed c_T) coming from $x \rightarrow (-\infty)$ is characterized by the amplitude (depending on the coordinate z) of the shear displacement field, assumed to be polarized along the y -axis (along the ridges). The ridged surface is assumed to be small deviations (which depend on the coordinate

x) from the regularly shaped surface which bounds outwardly the perturbed surface [defining the domain (D_0) , $z \in (-L_z/2, L_z/2)$]. The incident displacement field undergoes scattering on these irregularities, which therefore induces modes coupling inside the plate.

For this problem, the analytic procedure whereby one expresses both the perturbation of the incident field when propagating along the rough part of the plate and the field created by coupling due to the roughness is presented in a previous paper [1], this analytic procedure relying fundamentally on an integral formulation of the basic mathematical problem. The methodology used in this previous paper to solve the integral equation relies on an appropriate Green's function and a perturbation method (for small roughness) in the frame of a modal analysis, using a unique set of Neumann eigenmodes of the regularly shaped surface that bounds outwardly the perturbed surface of the plate.

The formalism gives analytic expressions for the coupled SH-waves which are considered, leading to expressions for the reflection coefficient at the input of the rough part of the plate and the transmission coefficient at its output (Appendix A1), which both depend on the parameters characterising the roughness and more specifically on the phase-matching (phonon relationship) between the wavenumbers (along the axis of the plate) of the propagating waves and the spatial periods of the roughness (the

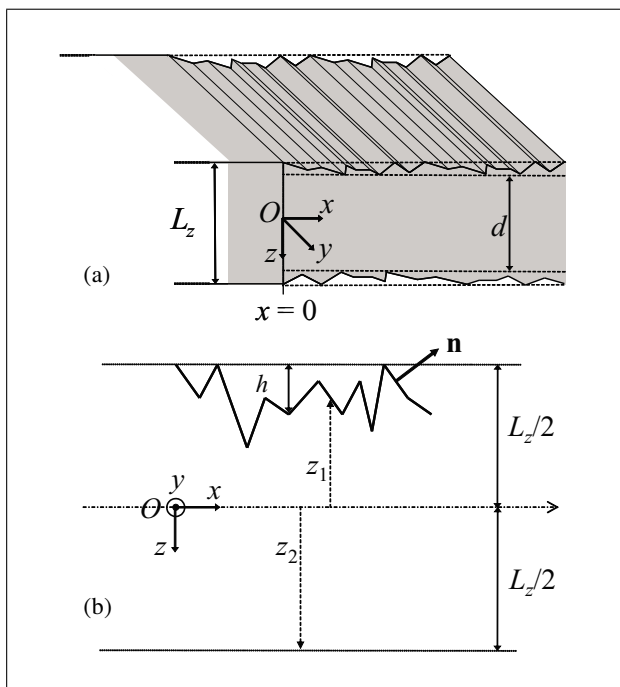


Figure 1. Sketch of the 2D waveguide with upper surface having small deviations (ridges). (a) General view and (b) zoom on the ridges.

ridges). Moreover, results obtained from an alternative analytical solution proposed in the literature [3, 4, 5, 6] (Appendix A2), which leads to almost accurate expressions for each mode when only two coupled modes are considered, are given to support the approach used in the present paper.

Being concerned herein by the use of the analytical approach mentioned above, not utilised until now, several results, yet typical of applications, are presented below and compared with some numerical (available in the literature) and experimental (given in the present paper) results. These results show that the method presented here could provide information on geometrical parameters characterising the profile of the roughness (this is of interest when other methods like optical methods cannot be used).

2. Phase matching effects

In each example chosen hereafter, the roughness is assumed to be either a periodically ridged surface or a more sophisticated surface which contains several periodic structures, always on one of the boundaries. Tables I and II give, for each figure presented below, the shape of the profile of the ridged surface, the values of its parameters (including its spatial periods Λ , its normalised depth h/L_z , and its total normalised length ℓ/Λ), the normalised thickness of the plate L_z/Λ , the adimensional frequency range $[f_1 d/c_T, f_2 d/c_T]$ considered [$d = L_z - \max[h(x)] \approx L_z$, see Figure 1a], the SH modes which satisfy the phase-matching (phonon relationship) in this frequency range, and the SH modes considered, namely incident (σ, m) and scattered (α, r) modes, m and r numbering

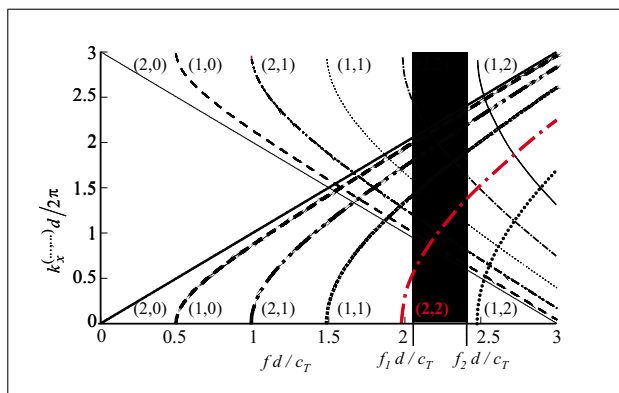


Figure 2. Dispersion curves (thick lines) and phonon (phase-matching) curves (thin lines).

the modes and σ and α denoting antisymmetrical (1) or symmetrical (2) modes. An example of dispersion curves and curves representing phase-matched relationship [1],

$$k_{x,m}^{(\sigma)} + k_{x,r}^{(\alpha)} - 2\pi/\Lambda = 0, \quad (1)$$

with $(k_{x,m}^{(\sigma)})^2 = k_T^2 - (k_{z,m}^{(\sigma)})^2$, $k_T = \omega/c_T$, and $k_{z,m}^{(\sigma)} = (2m + \delta_{\sigma 1})\pi/L_z$ (Neumann eigenvalues) is shown in Figure 2 (it corresponds to the results presented in Figure 3): in the frequency range considered ($f_1 d/c_T = 2.05$, $f_2 d/c_T = 2.45$), four strong couplings appear between the mode $(\sigma = 2, m = 2)$ and the modes $(\alpha = 2, r = 0)$, $(\alpha = 1, r = 0)$, $(\alpha = 2, r = 1)$, $(\alpha = 1, r = 1)$.

As a first example relying on the foregoing Figure 2 (a zoom in the frequency range of interest is given in Figure 3a), the transmission and reflection intensity coefficients respectively at the output and at the input of the roughness, obtained from the analytic procedure mentioned above (outlined in Appendix A1) when considering six modes in the calculus, are shown in Figure 3b for the configuration outlined in Tables I and II: transmission coefficient of the incident mode (2, 2) (upper curve, dashed-dotted line), and reflection coefficients (lower curves) of the counter-propagating, phase-matched modes (2,0) (solid line), (2,1) (dashed-double dotted line), (1,1) (dotted line), (1,0) (dashed line), as functions of the normalized frequency.

These curves show clearly that the energy transfers from the incident mode to each mode created by scattering on the ridges occur at the same frequency, when the corresponding phase-matched relationship is verified (Figure 3a). These results are coherent with those available in the literature (see for example [7, 8, 9]). Note that, owing to the roughness, the thickness of the plate is not known exactly, then, the calculated normalised frequency related to a phase-matching cannot be defined exactly.

In the following, in section 3 (Figures 4 to 7) the effects of the depth, the length, and the envelope of the roughness on the SH waves are analysed, and in section 4 (Figures 8 to 11) the behaviour of SH waves is investigated when the roughness contains periodic structures. Then, in section 5 (Figures 12, 13) and (Figure 14), comparisons with

Table I. Parameters of the ridges.

Figures	Shape profile	Normal. thickness L_z/Λ	Normal. depth h/L_z	Normal. length ϱ/Λ
3	Regularly distributed isosceles triangles	3	0.01	30
4	Regularly distributed isosceles triangles	2.5	(0.01,0.02)	50
5	Regularly distributed isosceles triangles	2.5	0.025	(0.65)
6, 7	Sinus, windowed	2.5	0.02	20
8, 9	Sinus, 2 periods	1.95	0.02	30
10, 11	Pseudo-random	(0.7,3) in (Λ_4, Λ_1)	(0,0.8)	(8,16) in (Λ_4, Λ_1)
12, 13	Regularly distributed trapezoidal grooves	1.67	0.01	40 and 100
14a	Regularly distributed isosceles triangles	0.68	0.04	30
14b	Regularly distributed isosceles triangles	0.68	0.04	20

Table II. Parameters of the SH-waves (modes).

Figures	Frequency range ($f_1 d/c_T, f_2 d/c_T$)	Phase-matched SH modes	SH modes considered	
			Inc. (σ, m)	Scattered (α, r)
3	(2.05,2.45)	(2,0) (1,0) (2,1) (1,1)	(2,2)	(2,0) (1,0) (2,1) (1,1)
4	(1.2,1.35)	(2,1)	(1,0)	(2,0) (2,1) (1,1)
5	(1.2,1.35)	(2,1)	(1,0)	(2,0) (2,1) (1,1)
6, 7	(1.65,1.9)	(1,1)	(2,1)	(2,0) (1,0) (1,1)
8, 9	(1.1,1.35)	(2,1)	(2,0)	(2,1) (1,0) (1,1)
10, 11	(0.5,0.85)	(2,0) (1,0)	(1,0)	(2,0) (1,0) (2,1) (1,1)
12, 13	(1.2,1.35)	(2,1)	(2,1)	(2,1) (2,0) (1,0) (1,1)
14.a	(0.28,0.40)	(2,0)	(2,0)	(2,0) (1,0)
14.b	(1,1.1)	(2,0)	(2,0) (2,2)	(2,0) (2,2) (1,0)

results obtained from the model outlined in Appendix A2 (two modes only) and with experimental results respectively, are presented.

3. Influence of the geometrical parameters of the grating

3.1. Influence of the depth of the ridges

Figures 4a and 4b show, for the same symmetrical sawtooth profile as the preceding one, the effects of the depth of the ridges on the reflection and transmission intensity coefficients respectively at the input and at the output of the roughness (the parameters are given in Tables I and II).

In Figure 4a, the transmission coefficient of the incident mode (2,2) and the reflection coefficients (lower curves) of the counter-propagating, phase-matched mode (2,1) are presented, as functions of the normalized frequency, for three values of the adimensional depth h/L_z : 0.010 (solid line), 0.015 (dashed line), 0.020 (dotted line). In Figure 4b, the reflection and transmission intensity coefficients are given as functions of the normalised depth of the ridges. As expected, these curves show clearly several features: first, the energy transfer from the incident mode to the scattered mode increases when the depth of the roughness increases; second, the phase-matched frequency decreases slightly when the depth of the roughness increases because the mean thickness of the plate decreases; third, the shape of the curves (Figure 4a) coincides with the square of a sinc function (see [1]); fourth, the sum of the

forward and the backward energy flux remains constant ($R + T \approx 1$); fifth, the width of the band gap increases when the depth of the roughness increases [10]. Note that these results are coherent with those obtained numerically for Lamb waves (see for example [11]).

3.2. Influence of the length of the grating

Figures 5a and 5b show the effects of the length of the ridges on the reflection and transmission intensity coefficients respectively at the input and at the output of the roughness, the other parameters being the same as the preceding ones (Tables I and II with $h/L_z = 0.025$). In Figure 5a, the reflection coefficients (lower curves) of the counter-propagating, phase-matched mode (2,1) and the transmission coefficient of the incident mode (1,0) are presented, as functions of the normalized frequency, for three values of the length ϱ/Λ (namely the number of teeth): 15 (solid line), 30 (dashed line), 45 (dotted line). Figure 5b, the reflection and transmission intensity coefficients are given as functions of the normalised length of the roughness. As expected, these curves show clearly several features: first, the energy transfer from the incident mode to the scattered mode increases when the length of the roughness increases; second, the phase-matched frequency does not depends on the length of the roughness; third, the shape of the curves (Figure 5a) coincide with the square of a sinc function (see reference [1]); fourth, the sum of the forward and the backward energy flux remains constant ($R + T \approx 1$). Once more, these results are coherent with those obtained numerically for Lamb waves (see for example [12]).

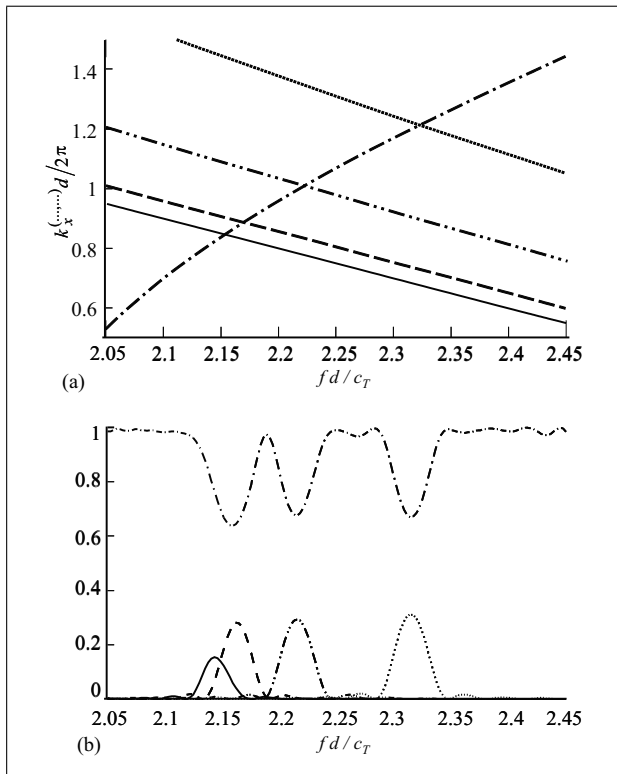


Figure 3. (a) Zoom of the dispersion and phase-matching curves (Figure 2) in the normalized frequency range (2.05,2.45). (b) Reflection and transmission intensity coefficients respectively at the input and the output of the roughness, as functions of the normalized frequency: reflection coefficients (lower curves) of modes (2,0) (solid line), (2,1) (dashed-double dotted line), (1,1) (dotted line), (1,0) (dashed line), and transmission coefficient of mode (2,2) (upper curve, dashed-dotted line).

3.3. Influence of the envelope of the grating

In the results presented above, the length of the roughness is just given by a truncation of its tails (the envelope of the roughness is given by a rectangular window of length ℓ). This leads to reflection and transmissions intensity coefficients expressed, as functions of the frequency, by the square of a sinc function [1], as shown in Figures 3, 4a, and 5a. Three smoothly tapered windows are considered hereafter. Ordering the windows chosen from the less to the more (smoothly) tapered, they are respectively: the rectangular window, the Hann window [half period ($0, \pi$) of sinus function], the Barlett window (triangle, using straight line for the taper), and the Blackmann window given by, in the interval ($0, \ell$):

$$0.42 - 0.5 \cos(2\pi x/\ell) + 0.8 \cos(4\pi x/\ell). \quad (2)$$

The Power Spectral Density (PSD) of these profiles for the windows considered, namely the Fourier transform with respect to the abscissa x of the autocovariance function of the adimensional depths of the roughness, as functions of the inverse adimensional spatial wavelength, are given in Figure 6, the profile of the ridges being assumed to be sinusoidal with a spatial period Λ . The effects of the windows of the roughness on the reflection [mode (1,1)] and

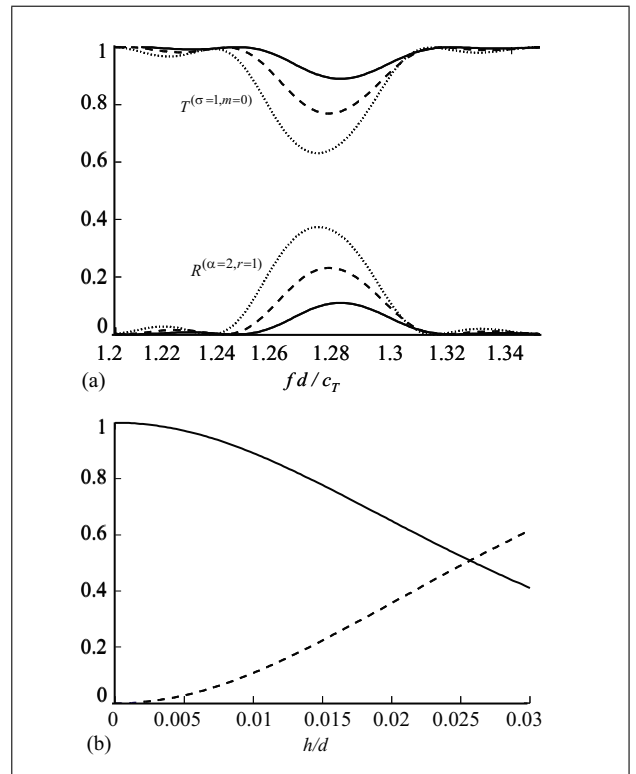


Figure 4. (a) Reflection coefficients (lower curves) of the counter-propagating, phase-matched mode (2,1) and the transmission coefficient of the incident mode (1,0), as functions of the normalized frequency, for three values of the normalized depth h/L_z : 0.010 (solid line), 0.015 (dashed line), 0.020 (dotted line). (b) Reflection and transmission intensity coefficients, as functions of the normalised depth of the ridges.

transmission [mode (2,1)] intensity coefficients are shown in Figures (7a) and (7b) respectively, as functions of the adimensional frequency (the other parameters are given in Tables I and II). The results are coherent with the properties of the windows.

4. Roughness containing periodic structures

In this section, the behaviour of SH waves is investigated when the roughness contains periodic structures (multiple spatial period, pseudo-random profile).

4.1. Roughness with multiple spatial periods

In the first two examples considered herein, the ridges are, respectively, a superposition of two sinusoidal distributions with spatial periods Λ_1 and Λ_2 given by

$$\frac{h}{4} [2 - \cos(2\pi x/\Lambda_1) - \cos(2\pi x/\Lambda_2)], \quad x \in (0, \ell), \quad (3)$$

and a juxtaposition of the same sinusoidal distributions expressed as

$$\frac{h}{2} [1 - \cos(2\pi x/\Lambda_1)], \quad x \in (0, \ell_0 < \ell), \quad (4a)$$

$$\frac{h}{2} [1 - \cos(2\pi x/\Lambda_2)], \quad x \in (\ell_0, \ell), \quad (4b)$$

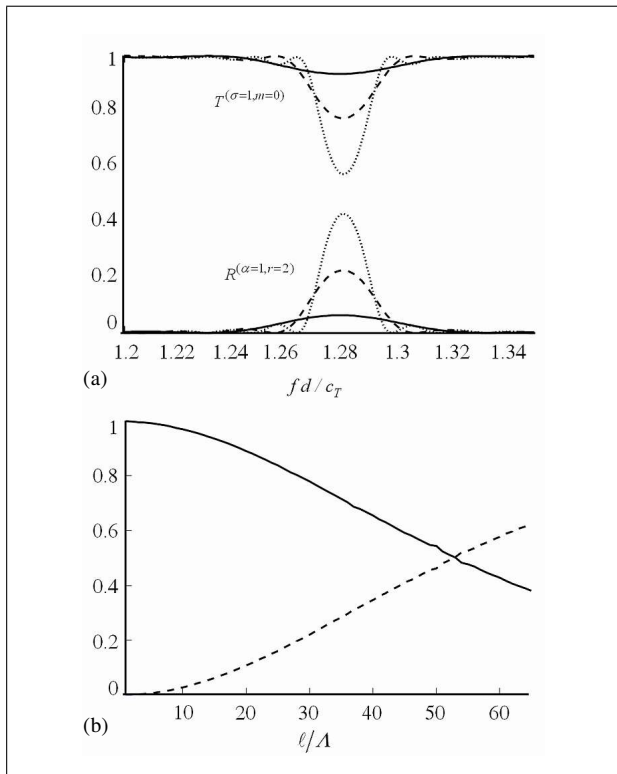


Figure 5. (a) Reflection coefficients (lower curves) of the counter-propagating, phase-matched mode (2,1) and the transmission coefficient of the incident mode (1,0), as functions of the normalized frequency, for three values of the length ℓ/Λ (namely the number of teeth): 15 (solid line), 30 (dashed line), 45 (dotted line). (b) Reflection and transmission intensity coefficients, as functions of the normalised length of the roughness.

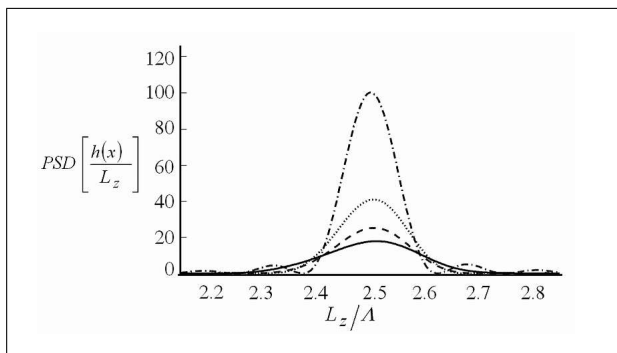


Figure 6. PSD of the roughness, functions of the inverse of the adimensional spatial wavelength, with sinusoidal ridges: for rectangular window (dashed-dotted line), Hann windows (dotted line), Barlett window (dashed line), Blackmann window (solid line).

where $\ell_0 = 15\Lambda_1$, $(\ell - \ell_0) = 16\Lambda_2$, and $(\Lambda_2 - \Lambda_1) \ll \Lambda$ with $\Lambda = (\Lambda_1 + \Lambda_2)/2$.

The PSD of these profiles, namely the PSD of the adimensional depths of the roughness, as functions of the inverse adimensional spatial wavelength, are shown in Figures 8a and 8b for the profiles given respectively by equations (3) and (4). It is noteworthy that the third spatial period Λ_3 which appears in Figure 8b is due to the super-

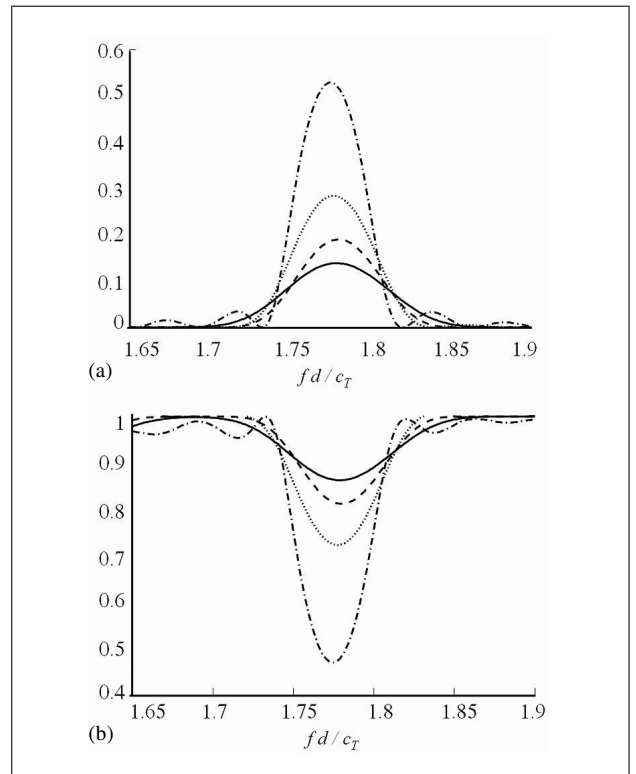


Figure 7. Effect of the window: rectangular window (dashed-dotted line), Hann windows (dotted line), Barlett window (dashed line), Blackmann window (solid line). (a). Reflection intensity coefficient of the incident mode (1,1) as function of the frequency. (b). Transmission intensity coefficient of the scattered mode (2,1) as function of the frequency.

position of the tails of the curves associated to the other periods (Λ_1 and Λ_2). The reflection and transmission intensity coefficients (obtained from the analytic procedure outlined in Appendix A1), respectively at the input and at the output of the roughness, are shown in Figure 9a for the profile 8a and in Figure 9b for the profile 8b, the configuration being outlined in Tables I and II: the lower curves (dashed lines) represent the reflection coefficient of the counter-propagating, phase-matched mode (2,1) and the upper curves (solid line) represent the transmission coefficient of the incident mode (2,0), as functions of the normalized frequency. These curves show clearly that the energy transfer from the incident mode to the mode created by scattering on the ridges occurs when the corresponding phase-matched relationship is verified for the corresponding frequencies, including the phase-matching linked to the third spatial period Λ_3 . These results are coherent with those available in the literature (see for example [6]).

4.2. Pseudo-random profile

In the next example, the roughness is assumed to have the pseudo-random profile shown in Figure 10a. Its PSD (Figure 10b) exhibits four spatial periods (usually, in practice, rough surfaces exhibit a limited number of dominant spatial periodicities). A zoom of the dispersion and phase-matching curves in the adimensional frequency range

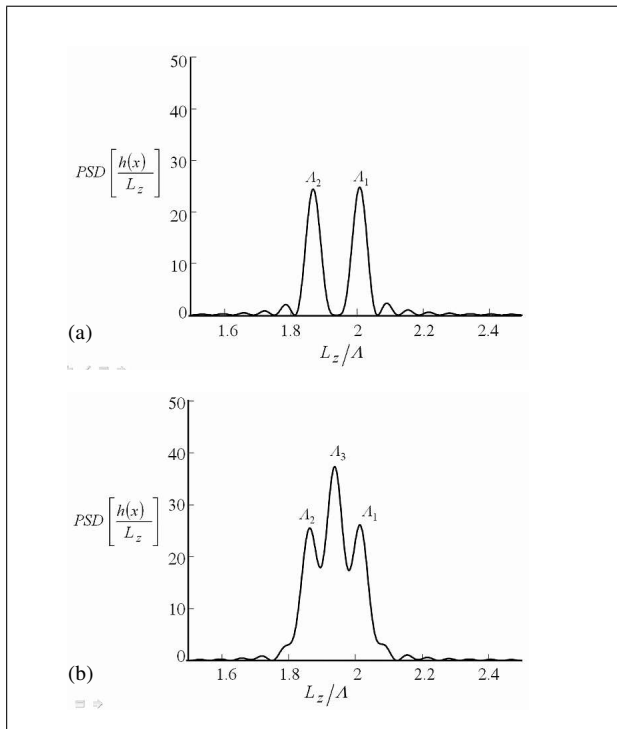


Figure 8. PSD of the adimensional depth of the roughness, as functions of the inverse adimensional spatial wavelength, for ridges with two sinusoidal distributions: (a) profile given by equation (3), (b) profile given by equation (4).

(0.5,0.85) is shown in (Figure 11a) and the reflection and transmission intensity coefficients (obtained from the analytic procedure outlined in Appendix A1), respectively at the input and the output of the roughness, are shown in Figure 11b, the configuration being outlined in Tables I and II. In both figures, the incident mode (1,0) is represented by the dashed-dotted line (forward propagative mode), the counter-propagative scattered mode (2,0) by the dashed line, the counter-propagative scattered mode (1,0) by a dotted line, and the dispersion curve of the phase-matched mode (2,0) by a solid line [the other modes (2,1) and (1,1) considered in the calculus are here evanescent modes]. These curves show clearly that the energy transfer from the incident mode to the modes created by scattering on the ridges (here the same mode as the incident one and another one) occurs when the corresponding phase-matched relationship is verified for the corresponding frequencies, i.e. here for three and four values of the frequency for the modes (2,0) and (1,0) respectively. These results show that conversions of SH waves can be predicted by computing the PSD of the roughness, and, conversely, information (i.e. spatial wavelength of periodic structures and their relative amplitudes) can be acquired through experimental results [13].

5. Comparison with analytical and experimental results

The remaining of the paper presents comparisons with results obtained from the model outlined in Appendix A2

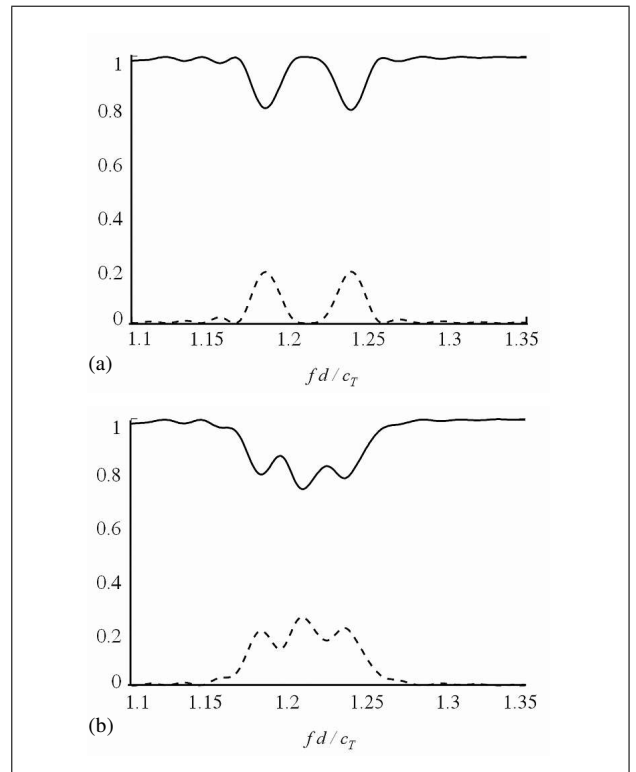


Figure 9. Reflection coefficients of the counter-propagating, phase-matched modes (2,1) (lower curve, dashed line) and transmission coefficient of the incident mode (2,0) (upper curve, solid line), as functions of the normalized frequency: (a) for the profile given in Figure (8a) and (b) for the profile given in Figure (8b).

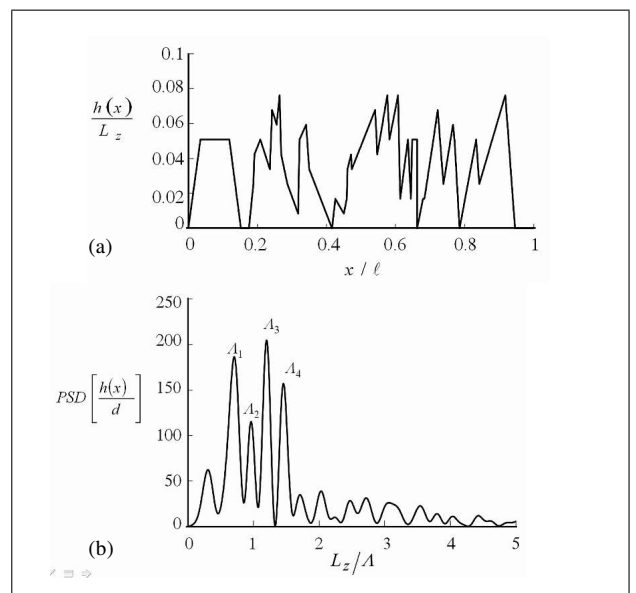


Figure 10. Pseudo-random roughness: (a) Pseudo-random profile, (b) PSD exhibiting four spatial periods.

(two modes only) and with experimental results respectively.

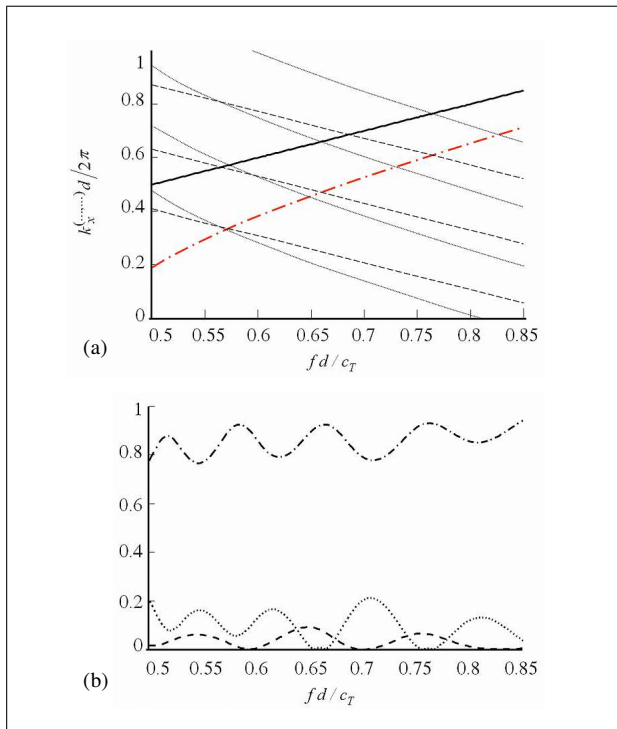


Figure 11. (a) Zoom of the dispersion and phase-matching curves in the adimensional frequency range (0.5,0.85). (b) Reflection and transmission intensity coefficients. In both figures: dashed-dotted line the incident mode [forward propagative mode] (1,0), dashed line the counter-propagative scattered mode (2,0), dotted line the counter-propagative scattered mode (1,0), dispersion curve of the phase-matched mode (2,0) by a solid line.

5.1. Comparison with the two-coupled modes theory

Figures 12 and 13 show, respectively for the normalized lengths ℓ/Λ equal to 40 and 100 (number of regularly distributed trapezoidal grooves), the results obtained for the reflection (a) and transmission (b) intensity coefficients as functions of the normalised frequency when only two modes are phase-matched, namely the incident one and the counter-propagating scattered one [both being the mode (2,1) here], four modes being considered in the calculation. In Figure 12, these results are calculated from both the analytical solution used in the present paper outlined in Appendix A1 (full lines) and an alternative analytical solution proposed in the literature [3] outlined in Appendix A2 (dashed-line), for the parameters given in Tables I and II. The curves show a good agreement between the analytical models, the slight deviation observed being probably due to the different natures of the approximations used to solve equations in each model. In Figure 13 the results are calculated from the alternative analytical solution (Appendix A2) only, because, in the stopband, the counter-propagative scattered wave reach the same amplitude as the incident one and thus the iteration process does not converges anymore in the other method (Appendix A1); but unfortunately this alternative method is limited to only two modes.

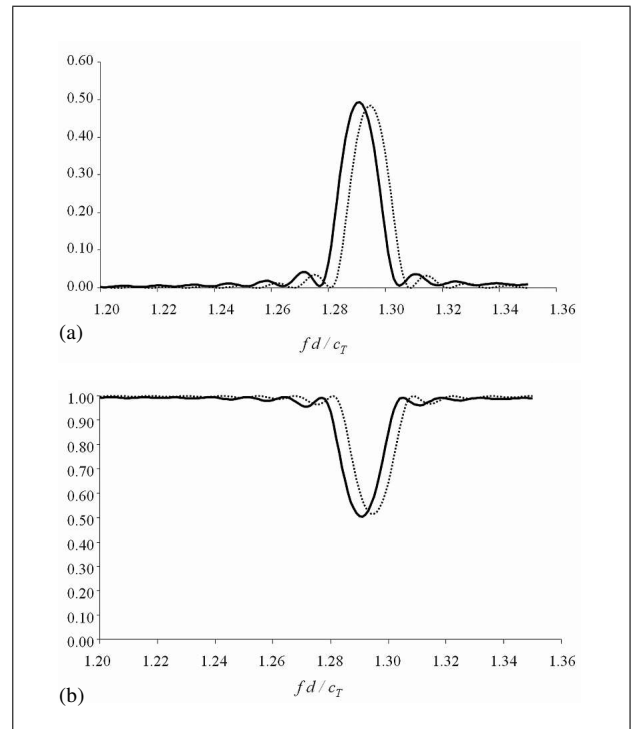


Figure 12. Reflection (a) and transmission (b) intensity coefficients as functions of the normalised frequency (40 grooves): (solid line) solution from model outlined in Appendix A1, (dashed line) solution from model outlined in Appendix A2.

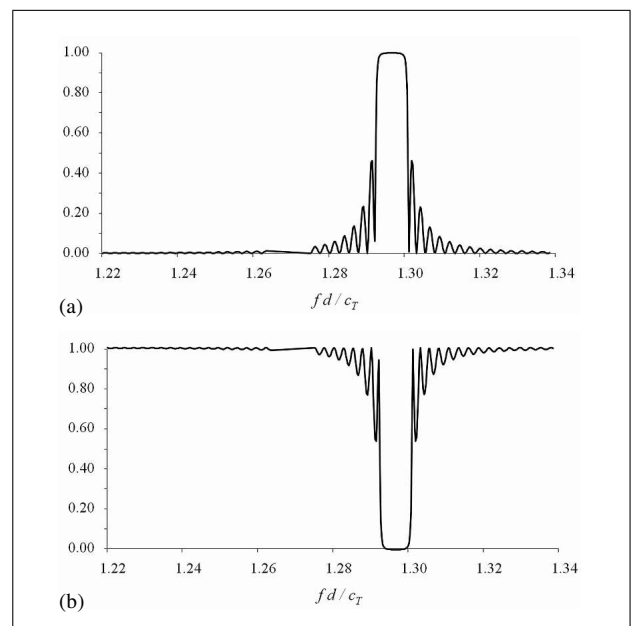


Figure 13. Reflection (a) and transmission (b) intensity coefficients as functions of the normalised frequency (100 grooves).

5.2. Comparison with results of measurements

The final part provides a comparison between analytical results obtained from the analytical model used in this paper (Appendix A1) and the experimental results obtained from the method presented in Appendix A3. Figures 14a and 14b show respectively the reflection and trans-

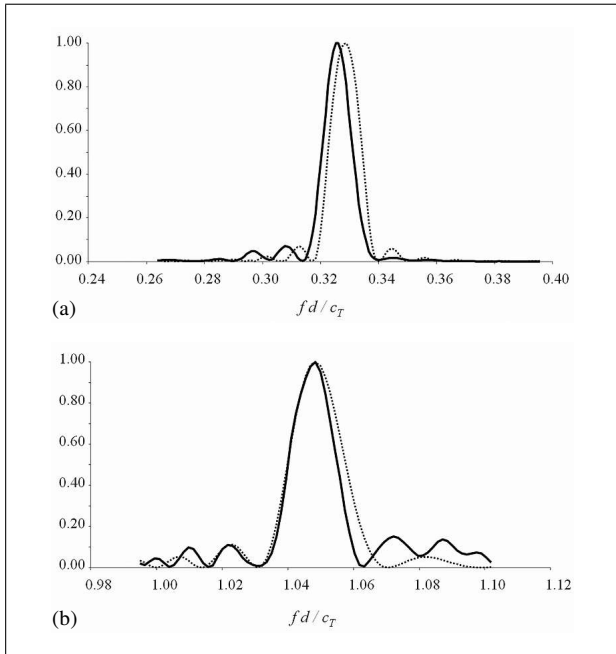


Figure 14. Reflection (a) and transmission (b) intensity coefficients, as functions of the normalised frequency, for the incident mode (2,0) phase-matched respectively with itself and the mode (2,2): theoretical result (dashed line), normalised experimental result (solid line).

mission intensity coefficients [theoretical curves (dashed lines), experimental curves (solid lines)] as functions of the normalised frequency when only two modes are phase-matched in the frequency range considered, namely the incident one (2,0) and respectively the counter-propagating scattered one (2,0) and the co-directional scattered one (2,2) [14, 15], three modes being accounted for in the calculation (see Tables I and II). Owing to the experimental technique, the experimental amplitudes of these coefficients are unknown. So, their maxima are here normalised with respect to the maxima of the theoretical results. Nevertheless, considering the shape of the curves, the agreement can be considered as excellent. It should be noted that the relative uncertainty $7 \cdot 10^{-3}$ on the experimental value of the shear velocity c_T can explain the slight frequency shift which appears between theoretical and experimental curves.

6. Conclusion

To conclude, it can be noted that the results analysed in this paper highlight several points. The analytical model used to describe the effects of the roughness is successful in relevant situations. It can handle a variety of realistic situations. While this modelling could appear somewhat cumbersome, the numerical calculations are in fact very simple and rapid to handle. This modelling would be effective in many applications even though it assumes that the roughness remains a small perturbation. Moreover, as mentioned in a previous paper [1], it is noteworthy that the theoretical results convey an interpretation of the physical

phenomena. Finally, it can be emphasized that, given the relative simplicity of the model used here to obtain the results, there is seen to be close agreement between these results and those available or expected (including results involving Lamb waves), thereby supporting this theoretical modelling.

Appendix

A1. The integral formulation and the iterative solution [1]

The displacement field $\hat{U}_y(x, z)$ in the domain (D) of the plate [the time dependence being given by $\exp(i\omega t)$] and the appropriate Green function in the domain (D_0) having a regularly shaped surface which bounds outwardly the perturbed surface of the plate, are both expressed as an expansion on the Neumann [in the domain (D_0)] eigenfunctions $\psi_m^{(\sigma)}(z)$, namely

$$\hat{U}_y(x, z) = \sum_{\sigma=1}^2 \sum_{m=0}^{\infty} \hat{A}_m^{(\sigma)}(x) \psi_m^{(\sigma)}(z), \quad (A1)$$

$$G(x, z; x', z') = \sum_{\sigma=1}^2 \sum_{m=0}^{\infty} [g_m^{(\sigma)}(x, x') \psi_m^{(\sigma)}(z')] \psi_m^{(\sigma)}(z), \quad (A2)$$

where the coefficients $A_m^{(\sigma)}$ are the unknowns of the problem, the coefficients $g_m^{(\sigma)}(x, x')$ being known ($\sigma = 1, 2$ respectively for antisymmetrical and symmetrical eigenfunctions). Straightforward calculation, starting from an integral formulation [1], yields the following relationship between the unknown coefficients $\hat{A}_m^{(\sigma)}$:

$$\hat{A}_m^{(\sigma)}(x) = \hat{F}_m^{(\sigma)}(x) + \sum_{\alpha=1}^2 \sum_{r=0}^{\infty} \left\{ \hat{H}_{rm}^{(\alpha\sigma)} [\hat{A}_r^{(\alpha)}(x)] + B_{rm}^{(\alpha\sigma)}(x) \hat{A}_r^{(\alpha)}(x) \right\}, \quad (A3)$$

where

$$\hat{F}_m^{(\sigma)}(x) = \int_{z_1}^{z_2} [g_m^{(\sigma)}(x, x') \psi_m^{(\sigma)}(z')] \hat{f}(z') dz' \quad (A4)$$

represents the effect of the incident field on the mode (m, σ),

$$\hat{H}_{rm}^{(\alpha\sigma)} [\hat{A}_r^{(\alpha)}(x)] = - \int_0^{\infty} \hat{A}_r^{(\alpha)}(x') \psi_r^{(\alpha)}(z'_1) \cdot \partial_{n'_1} \psi_m^{(\sigma)}(z'_1) g_m^{(\sigma)}(x, x') dx' \quad (A5)$$

represents the boundary modal coupling due to the shape profile of the roughness ($\partial_{n_1} = \mathbf{n}_1 \cdot \nabla$ denoting the normal derivative with respect to the outward normal \mathbf{n}_1),

$$B_{rm}^{(\alpha\sigma)}(x) = \left(\int_{-L_z/2}^{z_1} dz + \int_{z_2}^{L_z/2} dz \right) \psi_r^{(\alpha)}(z) \psi_m^{(\sigma)}(z) \quad (A6)$$

accounts for the depth of the roughness (bulk modal coupling), the endpoints z_1 and z_2 depending on the coordinate x .

Using an iterative method to express the amplitude of each mode $\hat{A}_m^{(\sigma)}(x)$, which assumes that the coupling function in the right hand side of equation (A3) is a small quantity compared to the source term $\hat{F}_m^{(\sigma)}$, thus the N th-order solution of this equation (A3) for $\hat{A}_m^{(\sigma)}(x)$ is written as

$$^{[N]}\hat{A}_m^{(\sigma)} = {}^{(0)}\hat{A}_m^{(\sigma)} + {}^{(1)}\hat{A}_m^{(\sigma)} + \dots + {}^{(N-1)}\hat{A}_m^{(\sigma)} + {}^{(N)}\hat{A}_m^{(\sigma)}, \quad (A7)$$

where

$${}^{(0)}\hat{A}_m^{(\sigma)}(x) = \hat{F}_m^{(\sigma)}(x) = \exp[-ik_{x_m}^{(\sigma)}x] \quad (A8)$$

denotes the zero order approximation (the solution without roughness), and where

$$^{[N]}\hat{A}_m^{(\sigma)}(x) = \hat{F}_m^{(\sigma)}(x) + \sum_{\alpha=1}^2 \sum_{r=0}^{\infty} \{ \hat{H}_{rm}^{(\alpha\sigma)} [^{[N-1]}\hat{A}_r^{(\alpha)}(x)] + B_{rm}^{(\alpha\sigma)}(x) [^{[N-1]}\hat{A}_r^{(\alpha)}(x)] \} \quad (A9)$$

denotes the N th-order perturbation expansion for $\hat{A}_m^{(\sigma)}$.

In the results presented in this paper, the amplitude of each mode $\hat{A}_m^{(\sigma)}$, governed by equation (A3), is truncated to the N th-order expansion (A9) with respect to the small surface perturbation, when the omission of the further term $^{(N+1)}\hat{A}_m^{(\sigma)}$ causes everywhere (i.e. for any value of x) a relative error lower than one-thousandth of the error caused when omitting term $^{(N)}\hat{A}_m^{(\sigma)}$, namely when $|^{(N+1)}\hat{A}_m^{(\sigma)}/^{(N)}\hat{A}_m^{(\sigma)}| \leq 10^{-3}$.

The reflection and transmission intensity coefficients are defined as

$$R_r^{(\alpha)} = \left| \overline{\phi}_r^{(\alpha)}(x=0) / \overline{\phi}_{\text{inc}} \right|, \quad (A10)$$

$$T_r^{(\alpha)} = \left| \overline{\phi}_r^{(\alpha)}(x=\ell) / \overline{\phi}_{\text{inc}} \right|, \quad (A11)$$

where $\overline{\phi}_r^{(\alpha)}(x)$ and $\overline{\phi}_{\text{inc}}$ are the time average energy flux of respectively the (r, α) reflected ($x=0$) or transmitted ($x=\ell$) mode and the incident modes.

A2. Two modes alternative solution [3]: Coupled modes theory

When a strong coupling between the incident mode (σ, m) and another mode (α, r) occurs in the frequency range of interest because of the phase-matching between both, for the spatial period Λ of a Fourier (sinusoidal) component of the roughness considered, equations (A3) can be solved directly for these two coupled modes, if the bulk modal coupling can be neglected (its effect is usually weak) and if the normal derivative of the Neumann eigenfunctions on the real boundaries can be expressed to the lower order approximation (small surface perturbation). For this spatial period Λ of the roughness, expression (A3) of the amplitude of the incident mode (σ, m) and the amplitude of the scattered mode (α, r) , where $j = 1, 2$ stand respectively

for a wave propagating in the same direction as the incoming wave (σ, m) and in the opposite direction, are respectively given by the following relations [equation (A3) for a Fourier component]:

$$\hat{A}_m^{(\sigma)}(x) = e^{-ik_{x,m}^{(\sigma)}x} \left[1 + \xi_{j,(m,r_j)}^{(\sigma,\alpha_j)} \int_0^x \hat{A}_{r_j}^{(\alpha_j)}(x') \cdot e^{(-)^j i(k_{x,m}^{(\sigma)} - 2\pi/\Lambda)x'} dx' \right], \quad (A12)$$

$$\hat{A}_{r_j}^{(\alpha_j)}(x) = (-)^j e^{-ik_{x,r_j}^{(\alpha_j)}x} \zeta_{j,(m,r_j)}^{(\sigma,\alpha_j)} \int_x^{\ell} \hat{A}_m^{(\sigma)}(x') \cdot e^{-i(k_{x,r_j}^{(\alpha_j)} + (-)^{j+1}2\pi/\Lambda)x'} dx', \quad (A13)$$

where $\xi_{j,(m,r_j)}^{(\sigma,\alpha_j)}$ and $\zeta_{j,(m,r_j)}^{(\sigma,\alpha_j)}$ are constant coefficients, where $x_1 = 0$ and $x_2 = \ell$, and where

$$(k_{x,m}^{(\sigma)})^2 = k_T^2 - (k_{z,m}^{(\sigma)})^2, \quad (A14)$$

with $k_T = \omega/c_T$ and $k_{z,m}^{(\sigma)} = (2m + \delta_{\sigma 1})\pi/L_z$ (Neumann eigenvalues).

The first derivative with respect to x of the set of equations (A12) and (A13) can be written as

$$\partial_x [\mathbf{X}(x)] = \mathbf{F}\mathbf{X}(x), \quad (A15)$$

where the matrix column $\mathbf{X}(x) = [S_m^{(\sigma)}(x) S_{r_j}^{(\alpha_j)}(x)]^T$ represents the amplitude of the modes considered when they are expressed as (T indicates the transpose operation)

$$\hat{A}_m^{(\sigma)}(x) = S_m^{(\sigma)}(x) e^{-i(k_{x,m}^{(\sigma)} - \delta_j)x}, \quad (A16)$$

$$\hat{A}_{r_j}^{(\alpha_j)}(x) = S_{r_j}^{(\alpha_j)}(x) e^{+i((-)^j k_{x,m}^{(\sigma)} - \delta_j)x}, \quad (A17)$$

and where the square matrix \mathbf{F} has the following property:

$$\exp[\mathbf{F}x] = \cos(\gamma_j x) \mathbf{I} + [\sin(\gamma_j x) / \gamma_j] \mathbf{F}, \quad (A18)$$

with

$$2\delta_j = k_{x,m}^{(\sigma)} + (-)^{j+1} k_{x,r_j}^{(\alpha_j)} - 2\pi/\Lambda \quad (A19)$$

(so-called detuning parameter), the parameters γ_j being known constants (\mathbf{I} is the unit matrix). Therefore, the solutions can be written as

$$\mathbf{X}(x) = \exp[\mathbf{F}(x - x_0)] \mathbf{X}(x_0), \quad (A20)$$

with, accounting for the conditions at the input $x_0 = 0$ and at the output $x_0 = \ell$ of the roughness,

$$\mathbf{X}(x) = \exp[\mathbf{F}x] \mathbf{X}(0) = \exp[\mathbf{F}x] \begin{bmatrix} 1 \\ 0 \end{bmatrix} \quad \text{for } j = 1, \quad (A21)$$

$$\mathbf{X}(x) = \exp[\mathbf{F}(x - \ell)] \begin{bmatrix} S_m^{(\sigma)} \\ 0 \end{bmatrix} = \exp[\mathbf{F}x] \begin{bmatrix} 1 \\ S_{r_j}^{(\alpha_j)} \end{bmatrix} \quad \text{for } j = 2. \quad (A22)$$

Table A1. Geometrical and physical parameters.

	ℓ (mm)	L_z (mm)	ρ (kg/m ³)	c_T (m/s)	h (mm)	Λ (nm)	(f_a, f_b) (kHz)	α (°)	f_e (Hz)
RC	126	2.88	2700	3080	0.12	4.2	(260,740)		300 to 450 by 1 kHz step
TC	148	5	2700	3080	0.20	7.4	(260,740)	7.5	670 to by 1 kHz step

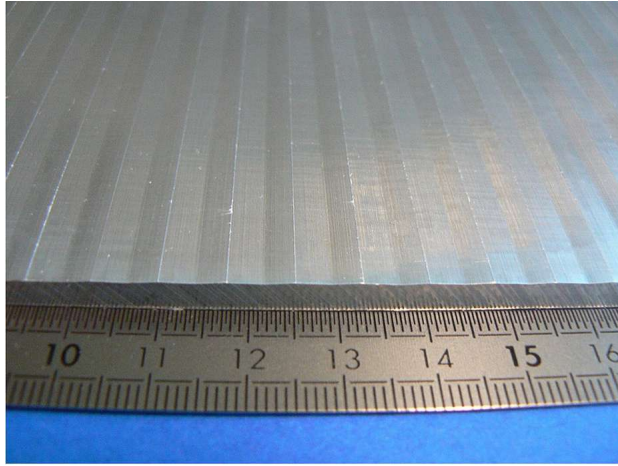


Figure A1. Photography of the corrugated interface of a sample.

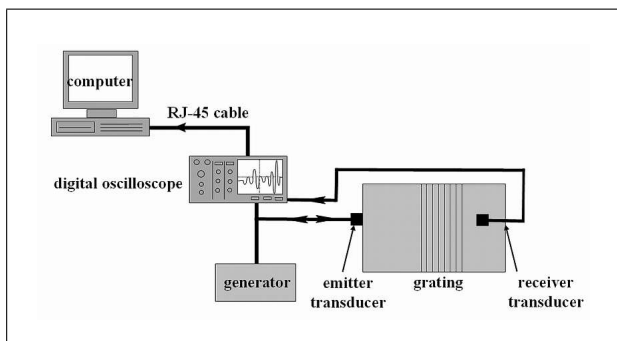


Figure A2. Block diagram of the experimental setup.

A3. Experimental method

The experimental setup [2] used for measuring the effects of couplings between contra-directional (Reflection Coefficient ‘‘RC’’) and co-directional SH-modes (Transmission Coefficient ‘‘TC’’) under a periodic distribution of ridges on a plate is presented in Figures A1 (photography of a ridged plate) and A2 (block diagram of the set-up). Transversely polarized, piezo-composite transducers are glued at the ends of the plate (over the thickness of the plate upstream and on the flat surface downstream) by means of a high-viscosity gel to ensure homogeneous applied shear stresses. The upstream transducer acts as both an emitter and a receiver for the same SH-mode (input and counter-propagating unique mode phase-matched with itself in the frequency range investigated), and the downstream receiving transducer is glued on a Plexiglas[®] wedge in order to detect another phase-matched mode created by coupling. The geometrical parameters of the plate (length of the ridged part ℓ and thickness L_z), the h physical param-

eters of the material of the plate (density ρ and SH-wave velocity c_T of aluminium), the geometrical parameters of the thirty (respectively twenty) isosceles triangular ridges (depth h and spatial period Λ), the -6 dB frequency bandwidth (f_a, f_b) of the transducers, the angle α of the receiving wedge, and the characteristics of the input signal (frequency f_e in a tone burst) are such as the modes involved in the measurements are (2,0) and (2,2) [these parameters are given in Table A1].

The excitation frequency f_e is tuned by 1 kHz step in the frequency ranges considered for the measurement of the reflection and the transmission coefficients respectively. For each value of the frequency, a signal averaging of 100 successive shots is carried out to improve the signal-to-noise ratio and a signal in the time domain of 200 μ s (25000 points) is registered. The same experimental procedure is applied to a plate without grating, providing a signal of reference for each frequency.

Fast Fourier Transform (FFT) is then calculated on each signal in the time domain providing a (f_e, f) matrix. The diagonal elements of this matrix constitute a vector \hat{A} whose each component represents the complex amplitudes of the FFT at a given excitation frequency. The ratio $\hat{A}\hat{A}^*$ (product of \hat{A} by its conjugate \hat{A}^*) with and without grating leads to the normalised reflection or transmission intensity coefficient (this ratio enables to cancel the effect of the frequency response of the transducers in their frequency passband).

Acknowledgement

Support from the CNRS through both the research group GDR 2501 and the ‘‘Fédération d’Acoustique du Nord Ouest’’ (FANO FR CNRS 3110) is gratefully acknowledged. The authors are indebted to Ministère de la Recherche that support the research studentship of the first author preparing his PhD-thesis that in part led to this paper. They wish also to express gratitude to Anne-Christine Hladky-Hennion (I.E.M.N. UMR-CNRS 8520) for helpful discussions.

References

- [1] T. Valier-Brasier, C. Potel, M. Bruneau: Shear acoustic waves polarized along the ridged surface of an isotropic solid plate: Mode coupling effects due to the shape profile. *J. Appl. Phys.* **108** (2010) 074910.
- [2] B. Morvan, A. Hladky-Hennion, D. Leduc, J. Izbicki: Ultrasonic guided waves on a periodical grating: Coupled modes in the first Brillouin zone. *J. Appl. Phys.* **101** (2007) 114906.
- [3] D. Royer, E. Dieulesaint: Elastic waves in solids II. Springer-Verlag, Berlin and Heidelberg, 1999.

- [4] C. Elachi: Waves in active and passive periodic structures. Review, *IEEE Trans. Ultrason. Ferroelectr. Freq. Control* **64** (1976) 1666–1696.
- [5] L. Brillouin: Wave propagation in periodic structures. Dover Publications Inc., 1956.
- [6] T. Valier-Brasier, C. Potel, M. Bruneau: Modes coupling of shear acoustic waves polarized along a one-dimensional corrugation on the surfaces of an isotropic solid plate. *Appl. Phys. Lett.* **93** (2008) 164101.
- [7] M. A. Hawwa: Acoustic/elastic stop-band interaction in waveguides involving two periodicities. *J. Acoust. Soc. Am.*, **102** (1997) 137–142.
- [8] Z. Tao, W. He, Y. Xiao, X. Wang: Wide forbidden band induced by the interference of different transverse acoustic standing-wave modes. *Appl. Phys. Lett.* **92** (2008) 121920.
- [9] Y. Yao, Z. Hou, F. Wu, X. Fu: The band structure and propagation property of Lamb waves in stubbed waveguides. *Wave Motion* **47** (2010) 343–349.
- [10] Z. Tao, W. He, Y. Xiao, W. Zhang, X. Wang: Sound transmission within the bragg gap via the high-order modes in a waveguide with periodically corrugated walls. *J. Appl. Phys.* **105** (2009) 123515.
- [11] M. Bavencoffe, A. Hladky-Hennion, B. Morvan, J. Izbicki: Attenuation of Lamb waves in the vicinity of a forbidden band in a phononic crystal. *IEEE Trans. Ultrason. Ferroelectr. Freq. Control* **56** (2009) 1960–1967.
- [12] D. Leduc, B. Morvan, A. Hladky, J. Izbicki: Interaction of Lamb waves with a grating composed of two spatial periodicities: Study in dual space. *NDT and E Int.* **42** (2009) 513–517.
- [13] J. C. Samuels: On propagation of waves in slightly rough ducts. *J. Acoust. Soc. Am.* **31** (1959) 319–325.
- [14] C. Elachi, C. Yeh: Mode conversion in periodically disturbed thin-film waveguides. *J. Appl. Phys.* **45** (1974) 3494–3499.
- [15] S. R. Seshadri: Coupling of guided modes in thin films with surface corrugation. *J. Appl. Phys.* **63** (1988) 115–146.